Effects of neutrino-electron scattering on neutrino transport in Type II Supernovae

Smit, J.M.; Cernohorsky, J.; van den Horn, L.J.; van Weert, C.G.

DOI
10.1086/177017

Publication date
1996

Published in
Astrophysical Journal

THE ASTROPHYSICAL JOURNAL, 460:895–901, 1996 April 1

EFFECTS OF NEUTRINO-ELECTRON SCATTERING ON NEUTRINO TRANSPORT IN TYPE II SUPERNOVAE

J. MARTIJN SMIT,[1] JAN CERNOHORSKY,[2] LEO J. VAN DEN HORN,[1] AND CHRISTIAAN G. VAN WEERT[1]
Received 1995 May 1; accepted 1995 September 18

ABSTRACT

We investigate the effects of neutrino-electron scattering on electron-neutrino transport during the collapse phase of a Type II supernova. Calculations of stationary state transport were performed on a 1.17 $M_\odot$ spherically symmetric infall model, with neutrino-electron scattering turned off and on. During the transport calculation, the stellar background is kept fixed in time. In this manner, we are able to isolate the effects of neutrino-electron scattering on neutrino transport alone.

We find that the inclusion of neutrino-electron scattering approximately doubles the emitted neutrino flux during infall. Neutrino-electron scattering increases the rate at which energy and lepton number are transferred from the matter to the neutrinos. However, the transfer of entropy to the matter increases in a large part of the collapsing core. We also discuss the equilibration of the neutrinos.

Subject headings: elementary particles — scattering — stars: interiors — supernovae: general

1. INTRODUCTION

Neutrino-electron scattering (NES) plays an important role during the collapse phase of a supernova (e.g., Bowers & Wilson 1982; Bruenn 1985; Myra et al. 1987; Bruenn 1988). As stressed by Bruenn (1985, 1988), NES is a crucial process determining the total amount of core deleptonization. During infall, neutrino-electron scattering occurs on very degenerate electrons which can only be *upscattered* to energies above the Fermi energy. The downscattered neutrinos escape more easily from the core because at low energies the neutrino mean free paths are longer. This enhances the lepton loss. In addition, NES was generally found to increase the matter entropy through the transfer of heat from the neutrinos to the matter. This leads to a higher free proton fraction (via the equation of state) and consequently higher electron capture rates. Another important aspect of NES was discussed by Bruenn & Haxton (1991). They investigated various neutrino-matter interactions and found NES to be the most effective mechanism for thermally equilibrating neutrinos and matter.

In a recent series of hydrodynamical collapse simulations, Mezzacappa & Bruenn (1993) made a detailed study of the NES effects in core collapse. They were able to solve the Boltzmann equation for neutrino transport and compared this approach with a multigroup flux-limited diffusion scheme (MGFLD). They made collapse runs with NES turned off and on and compared the results for several distinct central matter densities. Their work confirmed the picture sketched above, and they quantified the effects of NES to a greater extent. In their Boltzmann computations, the lepton fraction Y_l in the core center decreased from $Y_l = 0.385$ for a calculation in which NES was ignored to $Y_l = 0.345$ with NES included, both taken at a central density of $\rho_c = 10^{14}$ g cm^{-3}. They reported several significant differences between the results of their Boltzmann solver and MGFLD but found good agreement with respect to the overall effects: NES increases the emergent luminosity and decreases the average neutrino energy.

In this article we wish to isolate the effects of NES on neutrino transport alone and distinguish primary and secondary effects. We will also address the entropy exchange and the equilibration of neutrinos and matter attributable to NES. The impact of NES on transport alone can be distilled by considering stationary state solutions of the transport equation in which the dynamical feedback on the matter is ignored. When NES is included in a dynamic collapse calculation, matter evolves in a different way than without NES and one compares the neutrino fluid of different collapse models.

We have implemented NES in the numerical transport scheme of Cernohorsky & van Weert (1992, hereafter CW), which is a MGFLD approach. Momentum balance is achieved through the use of "artificial opacity" (Janka 1991). Our numerical implementation of NES is comparable to that of Bruenn (1985). The scattering kernel is expanded in a Legendre series in the scattering angle to first order. The integrals over the scattered neutrino energy that occur in the NES collision kernel are fully retained and not approximated as, for example, in the Fokker-Planck approach (Bowers & Wilson 1982; Myra et al. 1987).

2. NES IN NEUTRINO TRANSPORT

The inclusion of NES involves an additional contribution to the collision term in the Boltzmann equation:

$$\frac{1}{p^0}\, p^\mu \mathscr{F}_{\nu;\mu} = B(\mathscr{F}_\nu) = B_s(\mathscr{F}_\nu) + B_{\rm NES}(\mathscr{F}_\nu)\,, \qquad (2.1)$$

where B_s is the sum of neutrino-matter interactions that do not include NES, and $B_{\rm NES}$ is the contribution of NES alone (B is called $\omega^{-1}\, C$ in CW and is in units of cm^{-1}). In the present paper, B_s collectively contains absorption/emission and scattering on nucleons and nuclei, as listed in the appendix of CW. The distribution function $\mathscr{F}_\nu(x^\mu, p^\mu)$ is a function of spacetime coordinates x^μ and the neutrino four-momentum p^μ.

The NES algorithm is taken from Cernohorsky (1994), and in his notation the NES collision term is written as

$$B_{\rm NES}(\mathscr{F}_\nu) = \kappa^0_{\nu e}(\omega) - \mathscr{F}_\nu\, \kappa^e_{\nu e}(\omega) + \mathbf{\Omega}\cdot\tilde{\boldsymbol{\kappa}}_{\nu e}(\omega) - \mathscr{F}_\nu\, \mathbf{\Omega}\cdot\boldsymbol{\kappa}^f_{\nu e}(\omega)\,. \qquad (2.2)$$

[1] Center for High Energy Astrophysics (CHEAF), University of Amsterdam, Kruislaan 403, 1098 SJ Amsterdam, the Netherlands.
[2] Lawrence Berkeley Laboratory, University of California, 1 Cyclotron Road, Berkeley, CA 94720.

In this equation, $\omega = cp^0$ and $\mathbf{\Omega} = \mathbf{p}/p^0$. Expression (2.2) results from the expansion of the neutrino scattering rates into a linear polynomial in the scattering angle following Yueh & Buchler (1977). In a separate paper (Smit & Cernohorsky 1995), we show that a higher order expansion is not required at this stage in the collapse by explicitly calculating the quadratic terms and demonstrating that their contribution in electron-neutrino transport is negligible, as was already suggested by Yueh & Buchler (1977) and Mezzacappa & Bruenn (1993). Particle number conservation is imposed by relating the in- and out-scattering rates through the symmetries given in Cernohorsky (1994). Contrary to the implicit suggestion made in that article, the approach of Bruenn (1985) is formally correct and in principle does conserve lepton number. However, the use of the higher symmetry of the NES kernel discussed in Cernohorsky (1994) is computationally more efficient and more accurate.

By taking the first two angular moments of the Boltzmann equation, the angular dependence of $\mathscr{F}_\nu$ is integrated out and a set of two moment equations is obtained. These moment equations contain three moments of the distribution function:

$$e = \frac{1}{4\pi}\int_{4\pi} d\mathbf{\Omega}\mathscr{F}_\nu\,, \quad ef = \frac{1}{4\pi}\int_{4\pi} d\mathbf{\Omega}\mathbf{\Omega}\mathscr{F}_\nu\,,$$
$$e\mathbf{p} = \frac{1}{4\pi}\int_{4\pi} d\mathbf{\Omega}\mathbf{\Omega}\mathbf{\Omega}\mathscr{F}_\nu\,. \tag{2.3}$$

We assume spherical symmetry throughout, so that one must solve for $e(r, \omega), f = f_r(r, \omega)$ and $p = p_{rr}(r, \omega)$. In spherical symmetry, the contributions of the NES kernel to the moment equations are

$$\tfrac{1}{2}\int_{-1}^{1} d\mu B_{\rm NES} = \kappa^0_{\nu e} - e\kappa^e_{\nu e} - ef\kappa^f_{\nu e}\,, \tag{2.4}$$

$$\tfrac{1}{2}\int_{-1}^{1} d\mu\mu B_{\rm NES} = \tfrac{1}{3}\tilde{\kappa}_{\nu e} - ef\kappa^e_{\nu e} - ep\kappa^f_{\nu e}\,. \tag{2.5}$$

These must be added to the right-hand sides of equations (4.7) and (4.8) of CW, respectively. Each coefficient $\kappa_{\nu e}(\omega)$ is a functional of either $e(\omega)$ or both $e(\omega)$ and $f(\omega)$, which makes the moment equations integro-differential equations. We adopt the closure of Levermore & Pomraning (1981), $p = p(f)$, to close the set of moment equations.

3. NUMERICAL IMPLEMENTATION

The transport code solves the energy and momentum balance equations with equations (2.4) and (2.5) included when NES is turned on. The variables e, f, and p are computed on a spatial grid of NG = 140 points and NB = 30 energy bins. Special care was taken in the choice of these energy bins for the neutrino spectrum. Neutrino transport must be computed on a stellar grid that covers 6 orders of magnitude in mass density and up to 1 order of magnitude in matter temperature and electron degeneracy. The average neutrino energy decreases by almost an order of magnitude from the center out to the atmosphere, and these very different spectral shapes must be adequately covered by the selected energy bins. We chose energies to lie at the scaled roots of a 30th order Gauss-Laguerre polynomial. The Gauss-Laguerre roots were scaled such that the highest energy bin was 80 MeV. This is well above the Fermi energy of the degenerate electrons throughout the iron core (the Fermi energy at the center is 56 MeV).

NES was implemented in a semi-implicit scheme, in which the e, f, and p that multiply the $\kappa_{\nu e}$ values in equations (2.4) and (2.5) are computed at a new time step, but the coefficients $\kappa_{\nu e}$, which are functionals of e and f, remain at the old time. For the semi-implicit method, small time steps must be taken to avoid a large mismatch between the NES coefficients and the spectrum that is computed one step ahead. Such a mismatch would preclude stationary state solutions. We used 10 steps of 10^{-5} s when NES was switched on, and from thereon steps of 10^{-4} s were taken. A fully implicit method does not require the small time stepping, but the computational overhead is NB^2 times larger because one would also have to solve for e and f embedded in the coefficients $\kappa_{\nu e}$, and this couples all the energy bins at each time step. The need to turn to the fully implicit method might arise when numerical instabilities are encountered, but this never occurred in our calculations. In fact, inclusion of NES actually improves stability of the discretized set of equations because it smooths the neutrino spectra.

The transport routine makes use of a matrix inversion package of Blinnikov & Bartunov (1993) suitable for matrices of arbitrary sparseness.

4. TRANSPORT RESULTS

Transport runs were made against a stellar grid which we denote as M1. This model was extracted from a hydrodynamical collapse simulation of a 1.17 $M_\odot$ iron core inside an evolved Nomoto-Hashimoto (1988) 13 $M_\odot$ supergiant. The size of the iron core is $R = 460$ km. The background model M1 is shown in Figure 1, which also displays the model from which it was evolved. Model M1 (with a central density $\rho_c = 4.1 \times 10^{12}$ g cm^{-3}) is halfway in the collapse and will reach nuclear densities $\rho_{\rm nuc} = 2.7 \times 10^{14}$ g cm^{-3} in $\sim$4 ms real time. In our hydrodynamical calculation of M1, the neutrino transport contained NES and matter velocity–dependent terms. In the neutrino transport in this article, the matter velocity was ignored because its effect may draw attention away from NES. Only electron-type neutrinos were considered. Transport runs were made with NES both left out and included. In both cases, the transport was run until a stationary state was reached at which the time derivatives of the neutrino occupation density e and the first moment f had become negligible compared to other terms in the equations. The stationary state solutions of the transport equation without NES and with NES will be referred to as NES-OFF and NES-ON, respectively. NES was "switched on" with NES-OFF as initial profile. Several of the displayed figures exhibit, in addition to the NES-OFF and NES-ON states, an intermediate state at $t = 2.0 \times 10^{-4}$ s in the relaxation process from NES-OFF to NES-ON.

4.1. *Lepton Loss*

Figure 2 displays the local neutrino number luminosity

$$N_\nu = \frac{16\pi^2 r^2 c}{(hc)^3}\int_0^\infty d\omega\omega^2 e(\omega) f(\omega)\,, \tag{4.1}$$

in which $r = r(M)$ is the radius of the enclosed mass M, and c and h are the speed of light and Planck's constant, respectively. The number luminosity is substantially higher for model NES-ON than for NES-OFF at $M > 0.23\ M_\odot$ ($\rho < 1.4 \times 10^{12}$ g cm^{-3}). At the core edge, where $N_\nu(R)$ measures the deleptonization of the entire iron core, the

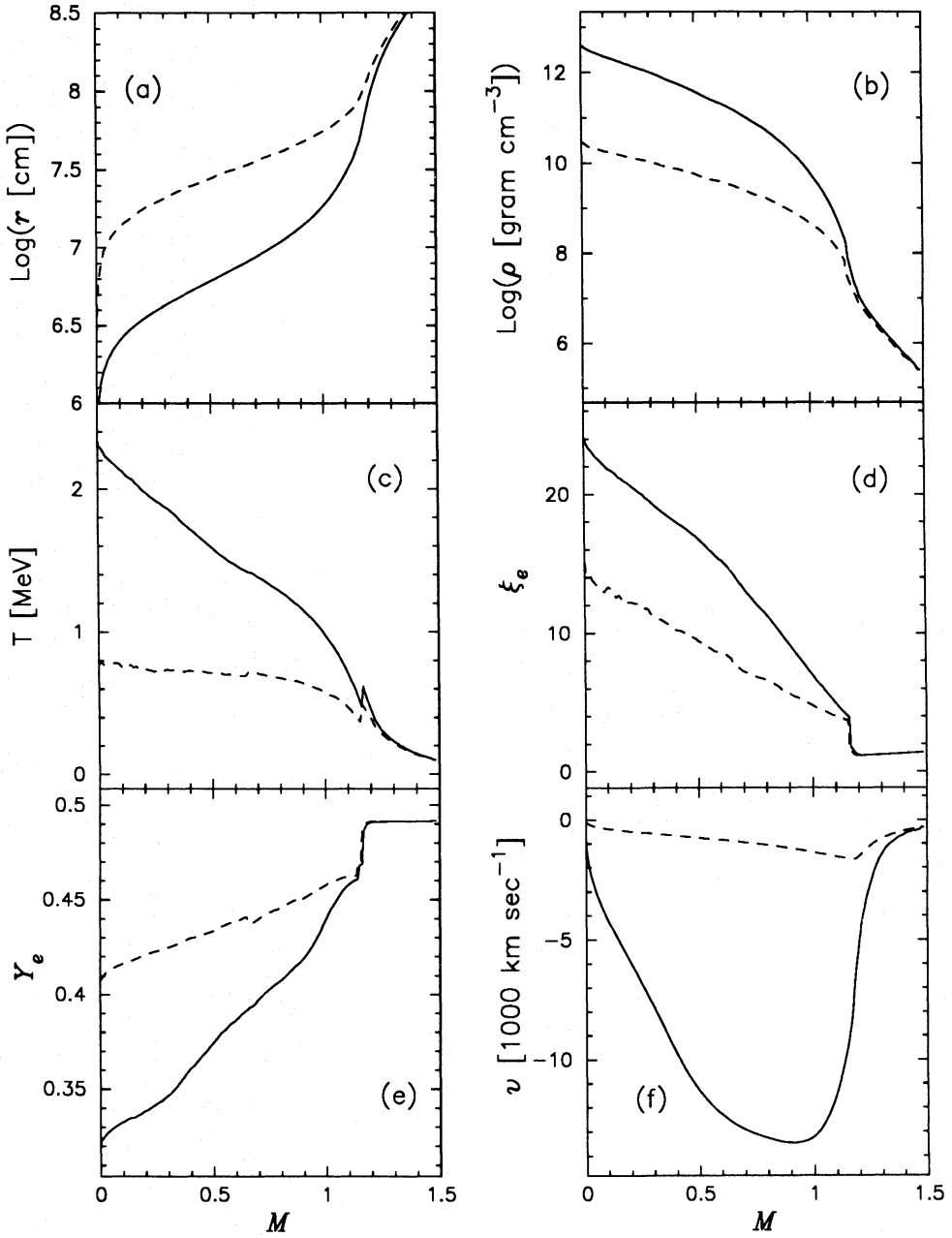

FIG. 1.—Background model M1 and the stellar model from which it has been evolved (*dashed line*). Displayed are: (*a*) log (*r*); (*b*) density log ρ; (*c*) temperature T; (*d*) electron degeneracy $\xi_e = \mu_e/kT$; (*e*) electron fraction Y_e; (*f*) matter velocity v.

lepton loss has more than doubled. Below $M = 0.23\ M_\odot$, the number luminosity is slightly lower for model NES-ON. The largest decrease of N_ν is $\sim 10\%$ at $M = 0.12\ M_\odot$. The decrease indicates that the mean free paths have become smaller in the inner core.

4.2. *Neutrino Fraction*

The neutrino fraction is given by

$$Y_\nu = \frac{4\pi}{n_b(hc)^3} \int_0^\infty d\omega \omega^2 e(\omega) , \qquad (4.2)$$

in which n_b is the baryon number density. From Figure 3 we see that Y_ν is larger throughout the star for the NES-ON model. The rapid rise of Y_ν above $M = 1.1\ M_\odot$ is a result of the baryon density "cliff" at that point, where the baryon density decreases more rapidly than $1/r^2$. The neutrino fraction in the transient state $t = 2 \times 10^{-4}$ s hardly differs from the NES-OFF state. This is an illustration of the fact that NES cannot change the lepton number directly. When NES is turned on, downscattering alters the neutrino spectrum (§ 4.4), but not the neutrino number. The NES-ON neutrino fraction then increases when neutrino absorption processes respond to the spectral change that NES has brought about.

4.3. *Transfer Rates*

In Figure 4*a* the lepton transfer rate is depicted. The rate SI (nucleon^{-1} s^{-1}) is the net transfer rate of lepton number from the matter to the neutrinos and is given by

$$\begin{aligned} SI &= \frac{c}{n_b h^3} \int d^3 p B(\mathcal{F}_\nu) \\ &= \frac{4\pi c}{n_b (hc)^3} \int_0^\infty d\omega \omega^2 \kappa_a(\omega)[b(\omega) - e(\omega)] \\ &= SI_\beta , \end{aligned} \qquad (4.3)$$

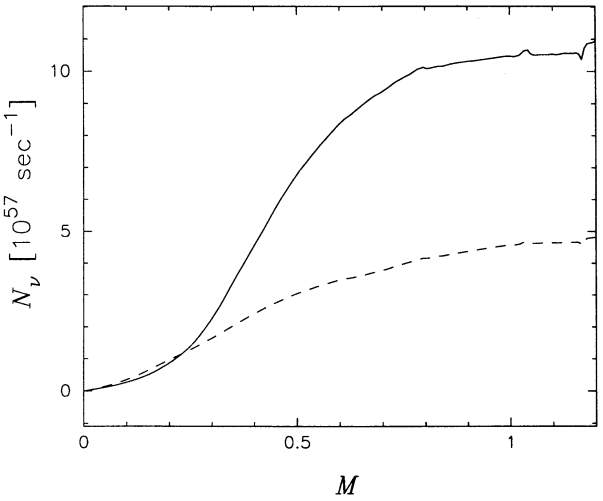

FIG. 2.—Neutrino number luminosity N_ν for model M1. Dashed line refers to the NES-OFF model; solid line refers to NES-ON.

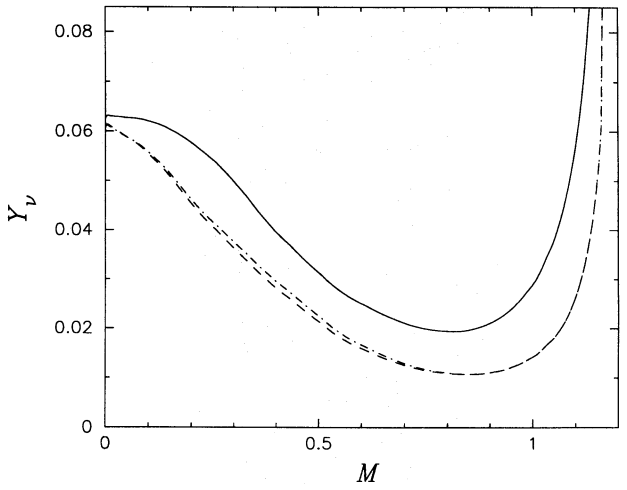

FIG. 3.—Neutrino number fraction Y_ν. Dashed line refers to the stationary state solution with NES ignored. Solid line refers to the stationary state solution with NES included. Dash-dotted line is the transient NES-ON neutrino state evolved for 0.2 ms.

where κ_a is the neutrino absorption coefficient and $b(\omega)$ is the equilibrium occupation density. The subscript β at the end of equation (4.3) indicates that only emission and absorption (β-processes) contribute to SI; NES, like other pure scattering processes, gives no contribution. In our calculations, the numericai contribution of NES to the rate SI was always less than 0.01% of the total, which quantifies the accuracy of our NES algorithm. Nevertheless, NES-ON displays a much higher SI than NES-OFF in a large region of the star, $0.2 < M < 0.7\ M_\odot$. It is this region that is mainly responsible for the enhanced neutrino number luminosity N_ν. In the region $M < 0.17\ M_\odot$ the NES-ON rate is somewhat smaller with respect to NES-OFF; there the neutrinos have equilibrated slightly (but note that even in the core center a nonzero SI remains). From the intermediate state in Figure 4*a* we see that initially a very strong transfer rate is present which, however, has not yet been able to significantly alter Y_ν (see the transient Y_ν in Fig. 3).

The energy transfer rate SQ (MeV nucleon^{-1} s^{-1}) is

$$SQ = \frac{c}{n_b h^3}\int d^3p\omega B(\mathscr{F}_\nu)$$
$$= \frac{c}{n_b h^3}\int d^3p\omega(B_s + B_{\rm NES})[\mathscr{F}_\nu]$$
$$= SQ_\beta + SQ_{\rm NES}\,, \qquad (4.4)$$

which contains a nonvanishing NES part. The other part involves only β-processes,

$$SQ_\beta = \frac{4\pi c}{n_b(hc)^3}\int_0^\infty d\omega\omega^3\kappa_a(\omega)[b(\omega) - e(\omega)]\,, \qquad (4.5)$$

and differs from SI_β by the weight of the neutrino energy. In Figure 4*b* the total rate SQ displays the same qualitative behavior as SI, being larger for model NES-ON in approximately the same spatial region. The contribution of NES, $SQ_{\rm NES}$, is shown in Figure 4*d*. It is seen that $SQ_{\rm NES}$ is negative, i.e., NES by itself transfers energy to the matter. In the outer regions of the star, beyond $M = 0.77\ M_\odot$, this makes the total rate SQ negative, but in the rest of the star SQ_β dominates over $SQ_{\rm NES}$ and the total rate SQ is positive there. In the NES-ON state, the total rate SQ has even increased in most of the star. The primary effect of NES to transfer energy to the matter, and its secondary effect, the mostly enhanced transfer of energy and particles to the neutrinos by β-processes, combine in the rate at which heat (or entropy) is transferred to the matter.

The heat transfer rate (MeV s^{-1} nucleon^{-1}) to the matter is

$$T\dot{s} = -(SQ - \mu_\nu SI)\,, \qquad (4.6)$$

with s the matter entropy per nucleon and μ_ν the chemical potential of the neutrinos. The heat transfer is shown in Figure 4*c*. Both profiles NES-ON and NES-OFF feature a cooling inner core region with a heated region above it. The region in which the matter is heated by the neutrinos is heated at a higher rate in the NES-ON state and also extends deeper inside the star.

The higher $T\dot{s}$ is not simply accounted for by the heating contribution of NES to that rate. Neutrino absorption and emission contribute through SI and SQ_β and those rates have increased in response to NES. The sign of $T\dot{s}$ in equation (4.6) is ultimately determined by the competing terms SI, SQ_β, and $SQ_{\rm NES}$. In the region $0.28 < M < 0.77\ M_\odot$, where SI, SQ, and $T\dot{s}$ all have increased, the relative increase of SI is larger than that of SQ, and consequently $T\dot{s}$ is higher there in the NES-ON state. The increase of the total rate SQ is limited by the negative contribution of $SQ_{\rm NES}$, whereas SI can grow with a larger factor because it does not contain a direct contribution of NES. For example, at $M = 0.4\ M_\odot$ NES has increased SI with a factor 3.3 and SQ_β with a factor 6.3, but the total SQ only increases with a factor 2.2, and altogether a higher heat transfer rate to the matter is established at this masspoint. However, NES tips the scale to a higher net transfer of heat to the neutrinos in the range $0.11 < M < 0.28\ M_\odot$. This region comprises a part in which SI and SQ have decreased as well as a part in which they have increased. And at $M > 0.77\ M_\odot$, the reduction of SQ and SI still results in a slightly higher $T\dot{s}$. Therefore, the NES-induced changes of the net particle and energy flows do not translate into an a priori higher, or lower, heat flow to the matter.

Neutrinos and matter also exchange momentum. We find that NES establishes at most a moderate $\sim$10% change in

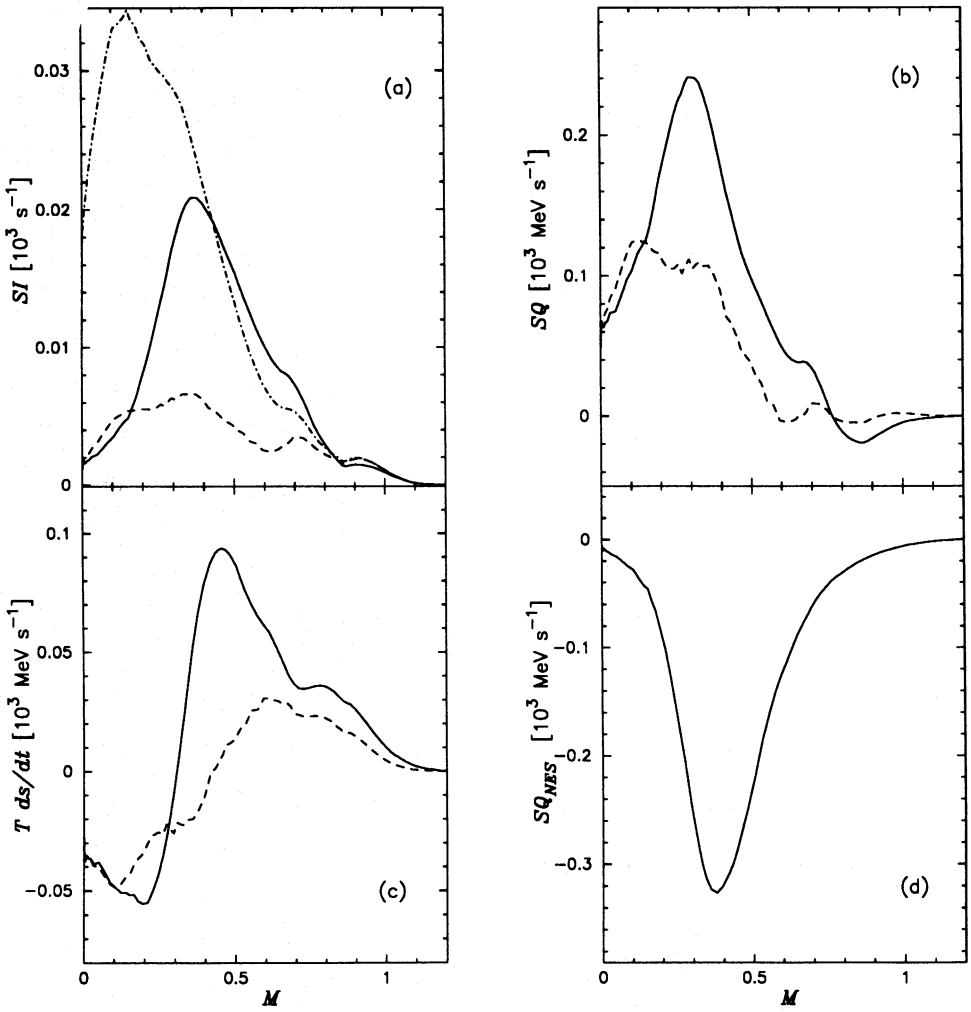

FIG. 4.—Transfer rates for model M1. Dashed line is the NES-OFF stationary solution, dash-dotted line is NES-ON evolved for 0.2 ms. Solid line is the NES-ON stationary state. (*a*) Total lepton transfer rate; (*b*) total energy number transfer rate; (*c*) entropy transfer rate (times temperature) $T\dot{s}$; (*d*) the NES-contribution to the energy transfer.

the total momentum transfer, but it contributes only $\sim 1\%$ directly.

4.4. *Occupation Density*

Next we focus on the spectral change that NES establishes in the region in which the NES-ON transfer rates are higher than the NES-OFF rates. In Figure 5 the occupation density $e(\omega)$ is displayed at $M = 0.34\ M_\odot$ ($\rho = 8.3 \times 10^{11}$ g cm^{-3}, $T = 1.8$ MeV). The figure shows the NES-OFF model, the intermediate model at $t = 2 \times 10^{-4}$ s after NES was switched on, and the NES-ON model. Also shown is the equilibrium (LTE) distribution $b(\omega)$ with $\mu_\nu(M) = 24$ MeV. The NES-OFF profile is characterized by low occupation at energies below 10 MeV. Compared with the equilibrium profile $b(\omega)$, the NES-OFF profile $e(\omega)$ seems to be very much out of equilibrium. The NES-ON profile has a very different shape. It is shifted to lower energies, and the low-energy states have become much more populated. The profiles at other positions in the star display the same behavior, and deeper inside the core the NES-ON low-energy states are fully occupied. We also see in this figure that at $t = 2 \times 10^{-4}$ s the population of low-energy states is in rapid progress: a large spectral change is taking place but without affecting the neutrino fraction Y_ν (see Fig. 3). The neutrino spectrum has only been shifted to lower energies with no change in the area underneath the curve $\omega^2 e(\omega)$. This area is proportional to Y_ν and is conserved by NES. At this stage in the evolution from NES-OFF to NES-ON, NES is therefore the only neutrino-matter interaction that has been effectively operative, and we observe its direct effect.

Looking at Figure 5, one might be tempted to state, since the occupation density $e(\omega)$ seems to approach $b(\omega)$ for the NES-ON model, that the neutrinos become equilibrated as a result of NES. In LTE, the neutrino distribution attains the equilibrium form $e(\omega) \rightarrow b(\omega)$ whereby SI and SQ vanish. But if we take another look at Figure 4, we see that, nonetheless, the NES-ON transfer rates SI and SQ have become much higher at this mass point. It is illuminating at this point to consider the spectral transfer rate SI_ω (s^{-1} nucleon^{-1} MeV^{-1}), defined by

$$SI \equiv \int_0^\infty d\omega SI_\omega \,. \tag{4.7}$$

It is displayed in Figure 6. The figure shows that the main contribution to SI for NES-OFF arises from neutrinos with energies between 5 and 40 MeV. For NES-ON, only neutrinos with energies between 15 and 40 MeV are relevant. Furthermore, above 27 MeV NES-OFF neutrinos add with a negative sign ($e > b$ in Fig. 5), whereas for NES-ON the

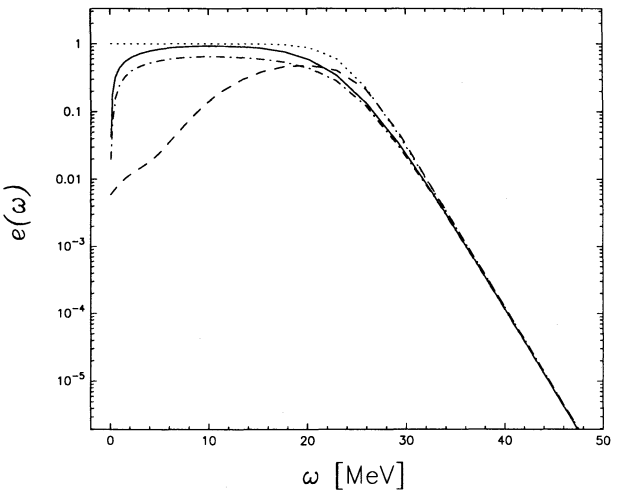

FIG. 5.—Neutrino occupation density $e(\omega)$ at a mass point $M = 0.34\ M_\odot$ ($\rho = 8.310^{11}$ g cm^{-3}). Dashed line is NES-OFF; solid line is NES-ON; dash-dotted line is the transient state at $t = 0.2$ ms. The dotted line is the equilibrium occupation density $b(\omega)$.

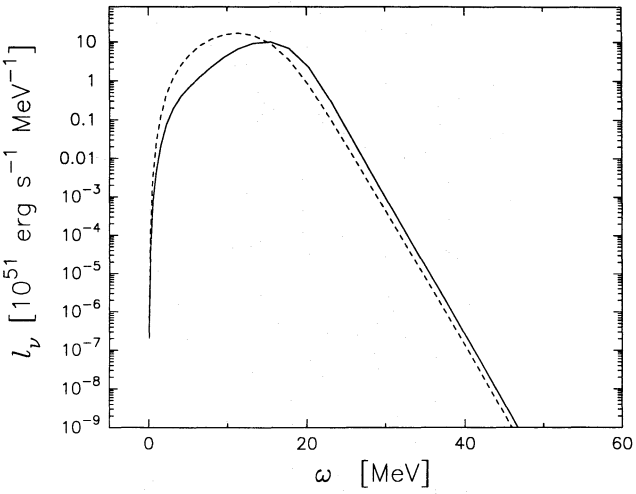

FIG. 7.—Emitted spectral neutrino luminosity $l_\nu(\omega)$. Dashed line is NES-OFF; solid line is NES-ON.

sign of SI_ω is positive at all neutrino energies. The equilibration of NES-ON neutrinos below 15 MeV is visible in Figures 5 and 6, but the plot of $e(\omega)$ fails to reveal the relatively more important disequilibrium of the NES-ON neutrinos above 30 MeV. Figure 5 is biased toward the equilibration of low-energy neutrinos whose weight is relatively unimportant in the transfer rates.

To conclude this section, we note that Figure 6 shows very clearly how the rate SI is indirectly increased by NES. The important positive contribution of high-energy neutrinos to SI in the NES-ON state indicates that the occupation density has been greatly reduced at those energies (from $e > b$ to $e < b$). The neutrino absorption rate, being proportional to $e(\omega)$, has decreased because high-energy neutrinos are downscattered before they can be absorbed. The neutrino emission rate is a thermodynamic function that does not depend on the neutrino state, NES-OFF or ON. With absorption diminished, the net neutrino production—the difference between emission and absorption—increases. The net energy transfer SQ also increases because a high-energy neutrino will essentially contribute to the energy reservoir with the energy it has after downscattering, instead of returning all its energy to the matter in an absorption.

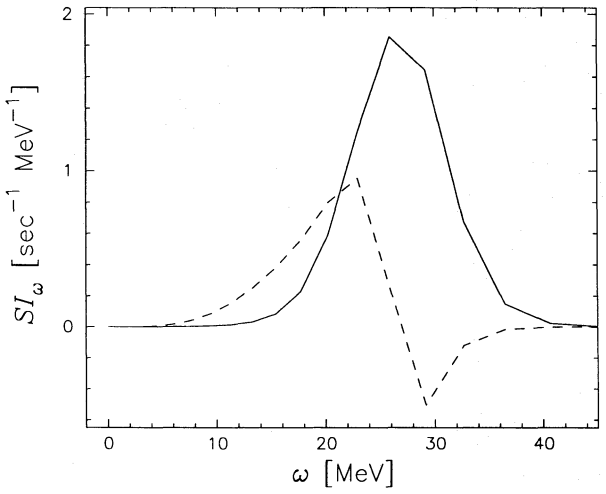

FIG. 6.—Spectral lepton transfer rate SI_ω at mass point $M = 0.34\ M_\odot$ ($\rho = 8.310^{11}$ g cm^{-3}). Dashed line is NES-OFF; solid line is NES-ON.

4.5. *Spectral Luminosity*

Finally, in Figure 7 we show the emergent luminosity spectrum l_ν (ergs s^{-1} MeV^{-1}), which is defined as

$$l_\nu = \frac{(4\pi)^2 cR^2}{(hc)^3}\,\omega^3 e(\omega) f(\omega)\,, \tag{4.8}$$

where R is the radius of the iron core. Below 15 MeV, the luminosity of the NES-ON model is nearly 1 order of magnitude higher than for NES-OFF. Above 15 MeV, the NES-ON luminosity is lower, but the difference with NES-OFF is smaller at higher energies. The average neutrino energy is lowered from 13 to 10 MeV when NES is included. The total area under the luminosity curves is the emitted energy per second L_ν and is 80% larger for model NES-ON. This is only slightly less than the increase found in $N_\nu(R)$ (see Fig. 2) and shows that the decrease of the average energy of the emitted neutrinos is more than compensated for by the enhanced net neutrino flux.

5. DISCUSSION

In our calculations, NES is responsible for a large amount of enhanced lepton emission from the collapsing iron core. If the deleptonization would proceed at the same rate in a dynamical run, then the shock that forms at bounce will lie deep inside the iron core, and this is unhealthy for any kind of supernova scenario that follows. The enhanced flux that we find as a result of NES, as well as the other reported effects, are not specific for the matter background we used in this paper. We also performed transport calculations with background models earlier and later in the infall phase, up to when the core reached a central density of $\rho_c = 10^{14}$ g cm^{-3}, and in all cases NES had the same qualitative effect on the neutrino transport quantities. Furthermore, the details of the neutrino transport, such as the closure $p(e, f)$ or the inclusion of matter velocity, did not change the relative importance of NES.

In an actual dynamical collapse situation the neutrino spectra do not reach a stationary state when their relaxation timescale is longer than the dynamic timescale at

which the matter background changes. The stationary state solutions presented here are therefore not to be taken as fully representative for the neutrino fluid at about the same matter configuration in a dynamic setting. Nevertheless, it is interesting to make a comparison of our results with the work of Mezzacappa & Bruenn (1993, hereafter MB). The matter background model M1 has been evolved (using dynamic neutrino transport) from the same initial iron core (Nomoto & Hashimoto 1988) as MB's. Our model M1, with a central density $\rho_c = 4.1 \times 10^{12}$ g cm^{-3}, is in between two snapshot models of MB whose central densities are $\rho_c = 10^{12}$ and $\rho_c = 10^{13}$ g cm^{-3} (we are referring to the models computed with NES included). This would preclude a direct comparison of the neutrino related quantities, but we are more concerned with the relative effects of NES. The largest differences are found between our and MB's emergent spectral luminosity $l_\nu(\omega)$ at high neutrino energies. Since MB found large discrepancies between the spectral luminosities that were computed with Boltzmann transport and the ones computed with MGFLD, we should only compare MGFLD. At neutrino energies below 15 MeV, the magnitude of our flux matches MB's for the $\rho_c = 10^{13}$ g cm^{-3} model. Below 15 MeV, the effect of NES on our luminosity agrees with MB, but at higher energies they find a much greater reduction of the spectral flux as a result of NES than we do. This difference can be attributed to the fact that we compare NES-ON and NES-OFF using one single background, which displays the effect of NES on the transport alone, whereas MB compare two different backgrounds, of which the density profile computed with NES was "less evolved," with lower densities than without NES.

Another difference is that our NES-OFF and ON fluxes at energies above 20 MeV are much lower than the MB fluxes for their $\rho_c = 10^{13}$ g cm^{-3} model. At 30 MeV, our fluxes are lower than those of MB by 1 order of magnitude. This has nothing to do with differences in the neutrino transport but rather reveals that at high energies our stationary state solutions fail to represent the dynamic neutrino state. In our computations, the inclusion of NES increases the neutrino fractions Y_ν throughout the stellar core. This occurs also in the MB model $\rho_c = 10^{12}$ g cm^{-3}, but quantitatively the Y_ν profile in M1 agrees more with the $\rho_c = 10^{13}$ g cm^{-3} model of MB. In our model, the emergent energy luminosities (not shown in our figures) are 10^{53} ergs s^{-1} with NES-OFF and 1.8×10^{53} ergs s^{-1} with NES-ON. These luminosities are larger than those of MB, but the relative effect of NES is of the same order. The energy luminosity profiles for M1 level off in the atmosphere (like N_ν; see Fig. 2), whereas the MB luminosities decrease in the outer atmosphere. This is indicative of the fact that MB luminosity profiles are dynamic. The luminosities are increasing fast in MB's successive snapshots, and the atmosphere lags behind a little. If we take this into account and compare our emergent luminosity with their peak luminosity for model $\rho_c = 10^{13}$ g cm^{-3}, then the magnitudes agree well. Although there are several differences between our work and theirs, the overall effects of NES are in good agreement.

Returning to our work, we conclude with the following remarks: The indirect effects of NES on neutrino transport were separated from the direct effects by considering several quantities on which NES has no direct impact, such as the neutrino fraction Y_ν and the lepton transfer rate *SI*. We have found that the total energy and lepton transfer to the neutrinos are greatly enhanced when NES is included. NES is a direct source of energy transfer to the matter, but the total net neutrino production is increased in response to neutrino downscattering. The higher energy and lepton transfer rates indicate that the neutrinos have moved away from LTE rather than toward it at this stage in the collapse. The neutrino spectrum in this respect was found to be a somewhat misleading measure of LTE. In our calculations, NES established a higher rate of heat (entropy) transfer to the matter in a large region of the collapsing core. The fact that NES alone transfers heat to the matter does not fully account for the higher total heat transfer. The indirect effects are such that β-processes transfer energy and lepton number at a strongly enhanced rate to the neutrinos. The combined effects nonetheless predominantly result in a net flow of heat to the stellar matter.

This work was supported by the Director, Office of Energy Research, Office of High Energy and Nuclear Physics, Division of Nuclear Physics, of the US Department of Energy under contract DE-AC03-76SF00098 at the Lawrence Berkeley Laboratory (LBL). This work was made possible in part by the hospitality and financial support of CHEAF and LBL, allowing for a visit of J. C. to CHEAF and of J. M. S. to LBL. The authors thank W. van Thor for useful remarks.

REFERENCES

Blinnikov, S. I., & Bartunov, O. S. 1993, A&A, 273, 106
Bowers, R. L., & Wilson, J. R. 1982, ApJ, 263, 366
Bruenn, S. W. 1985, ApJS, 58, 771
———. 1988, Ap&SS, 143, 15
Bruenn, S. W., & Haxton, W. 1991, ApJ, 376, 678
Cernohorsky, J. 1994, ApJ, 433, 247
Cernohorsky, J., & van Weert, C. G. 1992, ApJ, 398, 190 (CW)
Janka, H.-T. 1991, Ph.D. thesis, Max-Planck Institut für Astrophysik
Levermore, C. D., & Pomraning, G. C. 1981, ApJ, 248, 321
Mezzacappa, A., & Bruenn, S. W. 1993, ApJ, 410, 740 (MB)
Myra, E. S., Bludman, S. A., Hoffmann, Y., Lichtenstadt, I., Sack, N., & Van Riper, K. A. 1987, ApJS, 318, 744
Nomoto, K., & Hashimoto, M. 1988, Phys. Rep., 163, 13
Smit, J. M., & Cernohorsky, J. 1995, preprint
Yueh, W. R., & Buchler, J. R. 1977, ApJ, 217, 565